



HAL
open science

A cyclogenesis index for tropical Atlantic off the African coasts

Saïdou Moustapha Sall, Henri Sauvageot, Amadou Thierno Gaye, Alain Viltard, Pierre de Felice

► **To cite this version:**

Saïdou Moustapha Sall, Henri Sauvageot, Amadou Thierno Gaye, Alain Viltard, Pierre de Felice. A cyclogenesis index for tropical Atlantic off the African coasts. *Atmospheric Research*, 2006, 76 (2), pp.123-147. 10.1016/j.atmosres.2005.05.004 . hal-00561043

HAL Id: hal-00561043

<https://hal.science/hal-00561043>

Submitted on 27 Jul 2021

HAL is a multi-disciplinary open access archive for the deposit and dissemination of scientific research documents, whether they are published or not. The documents may come from teaching and research institutions in France or abroad, or from public or private research centers.

L'archive ouverte pluridisciplinaire **HAL**, est destinée au dépôt et à la diffusion de documents scientifiques de niveau recherche, publiés ou non, émanant des établissements d'enseignement et de recherche français ou étrangers, des laboratoires publics ou privés.



Distributed under a Creative Commons Attribution 4.0 International License

A cyclogenesis index for tropical Atlantic off the African coasts

Saïdou Moustapha Sall ^a, Henri Sauvageot ^{b,*},
Amadou Thierno Gaye ^a, Alain Viltard ^c, Pierre de Felice ^c

^a*Université Cheikh Anta Diop, Ecole Supérieure Polytechnique,*

Laboratoire de Physique de l'Atmosphère Siméon Fongang, Dakar, Sénégal

^b*Université Paul Sabatier, Observatoire Midi-Pyrénées, Laboratoire d'Aérodynamique, Toulouse, France*

^c*Institut Pierre-Simon Laplace, Ecole Polytechnique, Laboratoire de Météorologie Dynamique, Paris, France*

The westward moving Soudano-Sahelian mesoscale convective systems (MCS) frequently reach and cross the Atlantic Coast. At the end of their continental route, most MCS weaken and vanish over the ocean, near the coast, while others strengthen. The latter play an important part in the genesis of some Atlantic tropical cyclones. In the present paper, following the work of Gray (1977, 1979) [Gray, W.M., 1977. Tropical cyclone genesis in the western North Pacific. *J. Meteorol. Soc. Jpn.* 55, 465–482; Gray, W.M., 1979. Hurricanes: their formation, structure and likely role in the tropical circulation. *Meteorology over the Tropical Oceans*, D.B. Shaw, (Ed.), Roy. Meteorol. Soc., 155–218] and Gray et al. (1994, 1999) [Gray, W.M., Landsea, C.W., Mielke Jr., P.W., Berry, K.J., 1994. Predicting Atlantic seasonal tropical cyclone activity by 1 June. *Weather Forecast.* 9, 103–115; Gray, W.M., Landsea, C.W., Mielke Jr., P.W., Berry, K.J., 1999. Forecast of Atlantic seasonal hurricane activity for 1999. Dept. of Atmos. Sci. Report, Colo. State Univ., Ft. Collins, CO, released on 4 June, 1999], an index liable to be associated with the coast-crossing MCS cyclonic evolution is built. The data used in this work are observations by the Dakar-Yoff radar, reanalyses of NCEP/NCAR (National Centers for Environmental Prediction/National Center for Atmospheric Research), outgoing long wave radiation at the top of the atmosphere, and the resources of the National

* Corresponding author. Université Paul Sabatier, Observatoire Midi-Pyrénées, Laboratoire d'Aérodynamique, 65300 Lannemezan, France.

E-mail address: sauh@aero.obs-mip.fr (H. Sauvageot).

Hurricane Center data base. Several terms describing the variation of individual meteorological parameters are first analysed and then combined into an index of cyclogenesis or ICY. Combination of vertical vorticity at 925 hPa and potential vorticity at 700 hPa is notably found to be a good factor to discriminate between strengthening and weakening MCS over the near Atlantic. A good correlation between the ICY maximum and the beginning of the MCS cyclogenesis is observed. This index enables discrimination of the simultaneous presence of two separate cyclonic perturbations over the Atlantic. These results show that the sole variable ICY is useful to detect a cyclogenesis process in progress in a Sahelian MCS.

Keywords: Mesoscale convective systems; Cyclonic evolution; Cyclogenesis

1. Introduction

In the present paper, the concept of cyclogenesis refers to the growth of a tropical depression, then a tropical cyclone, from a pre-existing mesoscale convective storm (MCS—Frank, 1987). The study of cyclogenesis uses several dynamic and thermodynamic parameters. The processes involved in the cyclogenesis from a continental MCS and the respective weight of the various parameters in the associated enthalpy increase in the upper troposphere are not accurately understood. It is known, however, that this process creates convergence at low atmospheric level and divergence at upper level.

From a combination of significant atmospheric parameters, Gray (1977, 1979) has developed a climatological index to perform a climatology of cyclogenesis areas. This author provides a yearly forecast of cyclone activity over the Atlantic Basin (Gray et al., 1994, 1999). Using composite data obtained by radiosondes, McBride (1981) used Gray's index to study the regional differences of the tropical cyclone activity over the Northwestern Atlantic and Pacific. He shows that the evaporation rate is higher over the Pacific than over the Atlantic. Developed (i.e. pre-cyclones and mature cyclones) and non-developed systems for each basin are compared. The dynamic potential (defined from vertical vorticity, Coriolis parameter, and vertical wind shear) is found displaying significant differences while the thermal potential (defined from humidity, equivalent potential temperature, and oceanic energy) is almost stable. The Oceanic energy is linked with the water temperature higher than 26 °C over a depth of 60 m. It is expressed by:

$$E = \int_{Z_1}^{Z_2} \rho_w c_w (T - 26) dZ$$

where ρ_w is the density (in g cm^{-3}) and c_w is the specific heat (in $\text{cal g}^{-1} \text{ } ^\circ\text{C}^{-1}$) of sea water, T is the water temperature, and Z is the vertical coordinate with Z_1 corresponding to the surface level and Z_2 to the level -60 m or $T=26$ °C.

The area located off the Atlantic Coast of West Africa at the latitude of the Soudano-Sahelian Strip has been identified as an area of cyclogenesis. Rain in the Soudano-Sahelian Strip is associated with MCSs and notably squall lines (e.g. Laurent et al., 1998; Laing et al., 1999). Sahelian MCSs rapidly move westward over hundreds or thousands of kilometers. Frequently they reach the Atlantic Ocean at the end of their continental path, and when they

cross the Atlantic Coast, most of them weaken and disappear above the sea. Some systems strengthen, however, and move forward over the ocean where they play a major part in the birth of the tropical cyclones observed in late summer in the western Atlantic area (e.g. Gray and Landsea, 1992; Gray et al., 1994; Landsea et al., 1998; Thorncroft and Hodges, 2001). The powerful, frequent, and well-organized continental MCSs of the very wet years are correlated with a high number of cyclonic perturbations over the Atlantic Ocean. Hurricanes reaching the coast of the United States are thus markedly more numerous when wetter conditions with numerous MCSs are observed over the Sahel (Gray, 1990; Gray and Landsea, 1992; Gray et al., 1994; Landsea et al., 1998; Lawrence et al., 2001). The transition from MCS to cyclonic vortices has been discussed by Reed et al. (1977), Bartels and Maddox (1991), Harr et al. (1996), among others. Sall and Sauvageot (in press) have presented the case of Cindy observed in 1999 as an example of such a transition.

The processes that govern the dynamic of the cyclonic tropical disturbances have been addressed in many previous studies. Thorncroft and Hodges (2001) showed that there is a correlation between the number of easterly waves over West Africa and the number of tropical cyclones observed over the Atlantic. For example Lawrence et al. (2001), analyzing the 1999 cyclonic season, found that 11 of the 12 tropical cyclones recorded that year (i.e. 92%) originated from an easterly wave. Nevertheless, the transition between continental MCSs and the first cyclonic organization off the African coast is not well understood because it has rarely been observed and described.

Fig. 1 displays the trajectories of 289 convective storms observed in August 1994 from the Meteosat satellite infrared data and satisfying the following criteria assumed appropriate to select MCS: time life equal to or larger than 6 h and an equivalent area equal to or larger than a circle with a 100-km radius for a radiometric brightness temperature lower than $-40\text{ }^{\circ}\text{C}$. It shows that many westward moving Sahelian convective storms and MCSs reach the Atlantic Coast and that a significant fraction cross this line and travel over the sea.

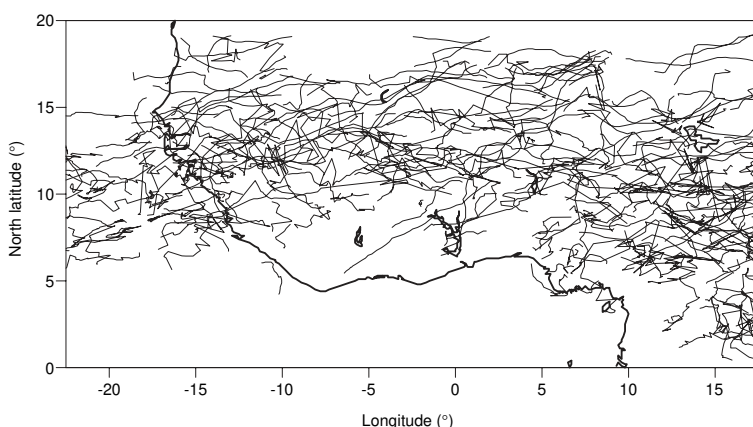


Fig. 1. Trajectory of 289 West African mesoscale convective systems observed in August 1994 and having both a lifetime longer than 6 h and an equivalent area equal or larger than a circle of radius 100 km for a brightness temperature lower than $-40\text{ }^{\circ}\text{C}$ (from Sall, 1997).

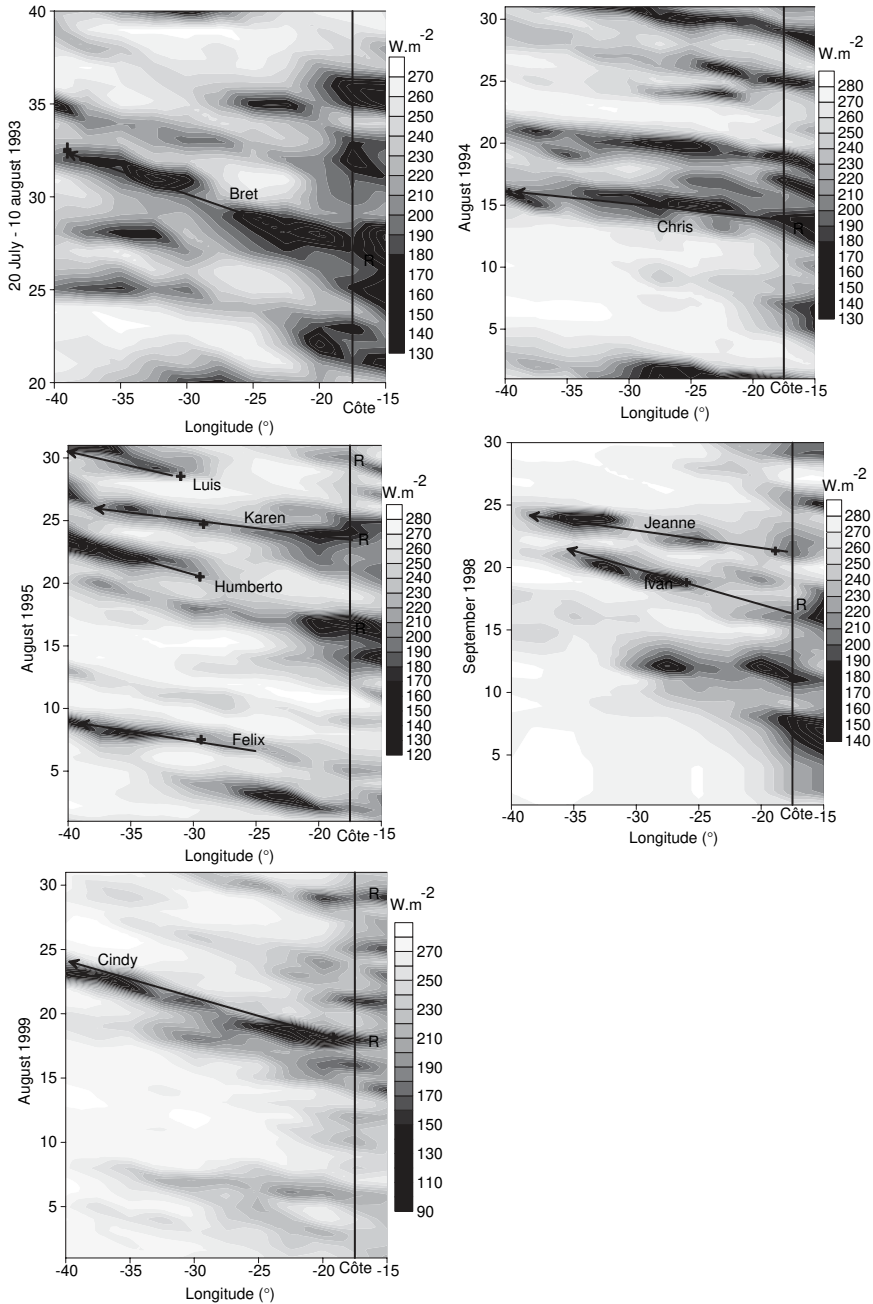


Fig. 2. Time-longitude diagram of the outgoing longwave radiation at the latitude of Dakar (15°N) for eight MCSs strengthening over the Atlantic ocean after coast crossing. Letter R points out the coast crossing of strengthening MCSs observed by the Dakar-Yoff radar. Arrow shows the MCS trajectory and (+) gives the time-longitude coordinates of each perturbation at the time of their classification as tropical depression by NHC.

To illustrate qualitatively the relation between the Atlantic cyclogenesis and the continent-originated MCSs, Fig. 2 presents a time-longitude diagram of the OLR (Outgoing Longwave Radiation) at the latitude of Dakar (15°N). Diverse summer periods corresponding to the presence of MCSs connected to a cyclogenesis west off the Africa coast are shown. Several continental MCSs are seen to be clearly related to a cyclogenesis. It seems that some cyclonic storms observed over the Atlantic Basin are not linked with an Africa-originated convection, for example cyclone Luis in 1995. The data from NHC (National Hurricane Center) show that the development of Luis is linked with an Africa-originated easterly wave. Other cyclones, such as Humberto observed in 1995, could originate from the split of a MCS.

The goal of the present paper is to propose an index trying to capture the coast crossing change leading either to the vanishing or to the strengthening and cyclogenesis of the Africa-originated MCSs. The present approach is clearly on the same line as previous works by Gray (1977, 1979) and Gray et al. (1994, 1999). The structure of a tropical cyclone, which is discussed in many papers (e.g. Gray, 1977, 1979; McBride, 1981; McBride and Zehr, 1981; Landsea et al., 1999), is out of the scope of the present paper. What is emphasized here is the transition of MCSs when crossing the African coast, an aspect which is not well known and rarely studied. Another original feature is the use of coastal radar data to discriminate between vanishing and strengthening coast-crossing MCSs.

Using the meteorological parameters assumed to have the best descriptive efficiency with respect to the MCS evolution, the following approach was used: for each parameter a factor called “parameter index” was tailored in such a way that this factor increases when the cyclogenesis conditions strengthen. In addition to the parameters considered by Gray, modified for some of them, other factors depending on the variability of precipitation in West Africa were defined. The proposed cyclogenesis index, ICY, is a combination of these parameter indices.

2. Data

The area considered in the present paper is the western part of the Sahelian strip, between about 12°N and 17°N , corresponding approximately to Senegal. It is a flat country without relief higher than 200 m over a distance larger than 500 km from the coast. Typically of the Sahelian climate, the rainy season is reduced to about four months, from early June to late September, when the latitude of the intertropical convergence zone (ITCZ) is higher than 12°N . The smoothed isohyets of the averaged annual rainfall accumulation display a strong meridional rainfall gradient (about 300 mm at 16°N and 1500 mm at 12°N). In the coastal area, Nzeukou and Sauvageot (2002) (NS 2002 hereafter) observe from radar data (see below) a land–sea gradient with less rainfall accumulation offshore than onshore, in such a way that resulting isohyets have an approximate North–East South–West orientation, as shown in Fig. 3. NS (2002) and Nzeukou et al. (2004) found, in spite of the strong space variation of the cumulative annual rainfall, that the rain rate (R) distribution over this area is approximately ergodic (i.e. the spatial and the temporal average and variance of R are equal). The mean conditional (when it is raining) climatological rain rate is around 5.1 mm h^{-1} . Consequently the rain duration

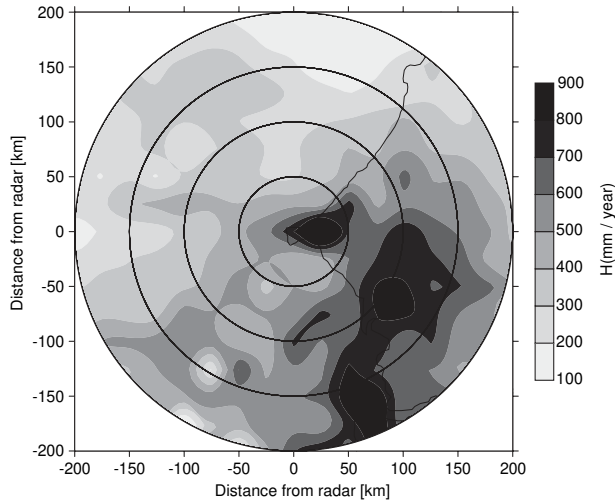


Fig. 3. Annual cumulative rainfall height averaged over seven years (1993–1999) calculated from the Dakar-Yoff radar data (from Nzeukou and Sauvageot, 2002).

observed in the Sahelian area is very short. Besides, the areal distribution of the rainfall accumulation displays a strong interannual heterogeneity. These results are supported by those of Kebe et al. (in press) which show that the ratio of the cloud top areas having an equivalent black body brightness temperature lower than -35°C to the radar-observed rain areas is constant throughout the entire observed area and equal to about 1.68.

The precipitation field in the coastal area is observed with a meteorological radar located at the Dakar-Yoff airport ($14^{\circ}34'\text{N}$, $17^{\circ}29'\text{W}$, altitude 30 m). It is a non-Doppler C band radar, with a peak power of 250 kW. The pulse repetition frequency is 250 Hz, the pulse width 3 μs , and the 3 dB beamwidth 1.3° . The data are in the form of PPI (Plan Position Indicator) and RHI (Range Height Indicator) of reflectivity, digitized on 8 bits, gathered with a time interval of 10–20 min and used over a circular area with a radius of 250–300 km (Fig. 3). It is calibrated and corrected for attenuation and variability of the reflectivity vertical profile using a probability matching method (Calheiros and Zawadzki, 1987) as described by NS 2002. These data are available for the 1993–1999 period.

Radar data have been used to select some cases of MCS undergoing important changes after coast crossing. Eight cases of strengthening and seven cases of weakening MCS were chosen. They are listed in Table 1 with the coast crossing date and, for the strengthening systems, the name of the associated tropical depression given to the system by the NHC.

Images of the infrared (IR) channel ($10.5\text{--}12.5\ \mu\text{m}$) from the geostationary satellite METEOSAT, at the time and space resolution of 30 min and $5\ \text{km} \times 5\ \text{km}$ (at the nadir), respectively, were also used to select additional cases of MCS strengthening and weakening after coast crossing in the aim to confirm the results obtained with the cases chosen from radar data. The high sampling frequency of the Meteosat images enables an accurate time-observation of the large-scale motion and evolution of the systems. The MCS tracking was performed by an automatic method derived from Arnaud et al. (1992)

Table 1

List of convective systems selected from radar data with respect to their evolution over the sea: either strengthening or weakening (and vanishing)

Evolution over the near Atlantic	Year	Identification code	Date of coast crossing (day/month)	Date of classification as tropical depression by NHC (day/month)	Name given by NHC to the tropical depression or hurricane
Strengthening	1993	93S	31/07	04/08	Bret
	1994	94S	10/08	16/08	Chris
	1995	95S1	16/08	22/08	Humberto
		95S2	25/08	26/08	Karen
		95S3	30/08		
	1998	98S	16/09	19/09	Ivan
	1999	99S1	18/08	19/08	Cindy
		99S2	29/08		
Weakening	1996	96W1	25/07		
		96W2	07/08		
		96W3	27/09		
	1998	98W	26/08		
	1999	99W1	27/07		
		99W2	29/07		
		99W3	14/08		

and Laurent (1996), using a brightness temperature threshold of -38 °C. This threshold was found to enable the best correlation between rainfall accumulation at ground level and the corresponding area of MCS cloud tops colder than -38 °C (Arkin, 1979; Richards and Arkin, 1981; Arkin and Meisner, 1987; among others). Kebe et al. (in press) confirm the validity of this threshold for West Africa. Only MCSs with a cold top area larger than an equivalent circle with a 100-km radius were considered (Mathon and Laurent, 2001). Selected MCSs also had to leave the African Coast between 12 and 17°N that is around the latitude of Dakar. The cold top area of the selected MCS over land and over sea, A_L and A_S , respectively, had to fulfill the following conditions:

- for the strengthening MCSs, A_S increasing up to $4/3 A_L$ west of the coast and held up to 25°W ,
- for the weakening MCSs, A_S decreasing to $2/3 A_L$ west of the coast and vanishing before reaching 25°W . Table 2 gives the number of MCS satisfying the above conditions from 1989 to 1998, for the months of July to September.

To elaborate the ICY cyclogenesis index, data on the outgoing long wave radiations (OLR) provided by the TIROS-NOAA (National Oceanic and Atmospheric Administra-

Table 2

Number of convective systems selected from the images of the IR channel of Meteosat between 1989 and 1998

	July	August	September	Total
Strengthening	15	21	08	44 (37.29%)
Weakening	16	33	25	74 (62.71%)
Total	31 (26.27%)	54 (45.76%)	33 (27.97%)	118

tion) satellite series were also used. The small values of the OLR flux coincide with convective systems with deep vertical development. Of course, satellite data are effective farther than radar data over sea.

Reanalyses by the NCEP/NCAR (National Centers for Environmental Prediction/National Center for Atmospheric Research) were used to describe the air motion, instability, and water distribution associated with the disturbance. These distributions, obtained from a combination between observations and general circulation models, provide good representations of the main characteristics of atmospheric circulation. Details about the models, assimilation technics, quality control, and validity limits can be found in Kalnay et al. (1996). A discussion on the validity of these reanalyses for West Africa is given in Diedhiou et al. (1999). Grist and Nicholson (2001) have used the reanalyses to emphasize the difference between four humid years (1958–1961) and four dry years (1982–1985) in the Sahelian area. Nicholson and Grist (2003) show the agreement between the meteorological profiles obtained by radiosondes and retrieved by the NCEP reanalyses over West Africa. The reanalysis provides air temperature, geopotential altitude, as well as the three components of wind velocity for 17 pressure levels in a grid mesh of $2.5^\circ \times 2.5^\circ$. It also provides the relative humidity between 1000 and 300 hPa.

Information on the characteristics of the tropical disturbances, notably their classification in the Saffir-Simpson code of intensity level (Simpson, 1974), provided by the NHC (National Hurricane Center) were used to follow and identify the time evolution of the systems over Atlantic.

3. Parameter indices and cyclogenesis index

3.1. Specific humidity

Humidity plays a central part in the convective system development and a high humidity concentration at low and middle tropospheric levels is favourable to cyclogenesis (e.g. Houze and Betts, 1981). For the Sahelian Africa, Deme et al. (2003) have shown the tight relation between the depth of precipitable water between 1000 and 300 hPa and the rainfall. Notably, they found that considering the precipitable water and convective inhibition (or CIN) parameters enable a better forecast of rainfall over the Sahel. Schematically, humidity originating in Gulf of Guinea is conveyed by convection in the middle tropospheric layer and then westward by the African Easterly Jet (AEJ). Water vapor is also injected in the middle and high tropospheric levels by the Indian monsoon dynamic process and conveyed westward by the Tropical Easterly Jet (TEJ) (De Félice et al., 1982, 1993; Lamb, 1983; Cadet and Nnoli, 1987; Diedhiou et al., 1999; among others). Humidity at middle level thus deserves to be used as a cyclogenesis parameter.

The index associated with the specific humidity Q is written:

$$IQ = \frac{1}{3} \sum_{p=600}^{850} Q_p \quad (1)$$

where p is the pressure level in hPa.

Gray (1977, 1979) also uses the middle tropospheric level to define an index from relative humidity. His index varies from 0 to 1 for a relative humidity between 40% and 70%.

3.2. Vertical wind shear

Vertical wind shear is an important dynamic parameter for convection development. It is necessary to maintain enthalpy and humidity in the convective column and this affects the tridimensional organisation of the systems (Gray, 1968; McBride and Zehr, 1981; Houze and Betts, 1981; DeMaria, 1996). The vertical wind shear is calculated between the two levels of the two strong wind axes, TEJ and AEJ. Several authors have calculated this parameter between 200 hPa (TEJ) and 900 hPa which is the mean condensation level in tropical oceanic regions (Gray, 1977; McBride and Zehr, 1981; DeMaria et al., 2001). The present work uses a vertical zonal wind shear index parameter built in such a way that it increases when the vertical shear of the zonal wind decreases because the decrease of vertical wind shear is favourable to the cyclogenesis. This index is defined as:

$$ICI = \frac{10}{\ln(|C_{is}U| + 10)} \quad (2)$$

where $C_{is}U$ represents the vertical shear of the zonal wind U between 200 and 700 hPa, that is $U_{200}-U_{700}$ and \ln is the Neperian logarithm. When the vertical shear of the zonal wind decreases and tends towards zero, index ICI increases and tends towards 4.34.

The wind shear index of Gray (1977), written $1/(S_z+3)$ where S_z is the vertical wind shear between 900 and 200 hPa, shows important variation around -3 which can overweight the correct contribution of vertical wind shear in the cyclogenesis index in some areas.

3.3. Equivalent potential temperature and warming

Several authors have stressed the descriptive interest of equivalent potential temperature (θ_e) due to tight relation with convective activity (Emanuel et al., 1993; Thorncroft et al., 2003). From BOMEX (Barbados Oceanographic Meteorological Experiment) data, Aspliden and Adefolalu (1976) have emphasized the relation between θ_e and convection from a classification of various convective modes. For conditions favourable to cumulonimbus development, the minimum of θ_e is between 700–500 hPa. Using radiosonde data, Sarr et al. (1995) have shown that just before the advent of squall lines, vertical profiles at Dakar are characterized by a positive vertical gradient of the humid and saturated static energy at low tropospheric level (what corresponds to a decrease of θ_e), with high values near the ground and minimum between 700 and 500 hPa. On the other hand, for squall lines decaying before reaching Dakar, the vertical gradient of the humid and saturated static energy at Dakar is negative or slightly positive (which corresponds to an increase of θ_e) and the minimum of θ_e is between 900 and 700 hPa.

Inspired by the classification proposed by Aspliden and Adefolalu (1976) and the results of Sarr et al. (1995), Deme et al. (2003) have built an index named ASP (for

Aspliden) defined as the difference between the minimum of θ_e (between 1000 and 600 hPa) and the mean of its relative maximum, usually around 1000 and 300 hPa. These authors show that this index is among the best predictors of rain at Dakar. They suggest that the maximums of ASP could be compared to the instability areas linked to the AEJ observed by Diedhiou et al. (1998) from potential vorticity. Aspliden and Adefolalu (1976) have shown that the vertical profile of θ_e depends on convection.

In this work, the level 600 hPa where the minimum of θ_e is observed for deep convection by Aspliden and Adefolalu (1976), Sarr et al. (1995), and Deme et al. (2003) is used. The Gray's index has thus been written on the form:

$$IT_e = \theta_{e1000} - \theta_{e600} \quad (3)$$

where θ_{e1000} and θ_{e600} are θ_e at 1000 and 600 hPa, respectively. The lower values of IT_e correspond to the stronger convection.

To IT_e measuring convective instability, we have added another parameter to quantify the warming inside the storm. Cyclogenesis analyses have shown that, in all the cases, a warming is observed in the upper layer of a MCS during its transition toward a tropical depression organization. When such a warming is not observed, cyclogenesis does not occur (Gray, 1979; McBride, 1981). From the difference between temperature inside a convective system and the environmental temperature, McBride (1981) shows that, over the Atlantic, horizontal temperature gradient is strong in the upper layer, around 300 hPa for systems where cyclogenesis is in progress and lower elsewhere. Consequently, the temperature difference between the d day and the previous day ($d - 1$), at 300 hPa, were taken as additional index, namely:

$$IRE = (T_{300,d} - T_{300,d-1}) + 5. \quad (4)$$

Number 5 is an invariant added in order to avoid a change of the cyclogenesis index sign. The warming parameter was not considered in Gray's climatologic index.

3.4. Vertical potential vorticity

Potential vorticity was widely used to discuss cyclogenesis starting processes (Balasubramanian and Yau, 1996; Wayne and Colucci, 1996). Charney and Stern (1962) have shown that a necessary condition of internal instability in a jet is that the sign of the potential vorticity gradient change on an isentrop or be inverted with respect to the temperature gradient above the surface. Using these conditions, Diedhiou et al. (1998) have shown the presence of instability areas on the African Continent. As a parameter, the potential vorticity includes information both on the mass distribution and on the swirling character of the atmospheric air (Molinari et al., 1994; Arbogast, 2002). Potential vorticity conservation of an air volume moving from a region characterized by a strong static stability towards a region where the static stability is weaker imposes a vorticity increase by stretching.

Well before Diedhiou et al. (1998), Burpee (1972) has shown that the potential vorticity gradient associated to the AEJ and the temperature gradient in the middle tropospheric layers satisfy to the criterium of instability favourable to easterly wave development. They contribute to the birth of tropical cyclones over the Atlantic from the activation of West

African MCS (Thorncroft et al., 2003). Arbogast (2002) shows that cyclogenesis results from interaction between preexisting coherent structures, the precursors, which can be described using the potential vorticity as only variable. In fact, at the synoptic scale, temperature and wind field can be retrieved from the only data of potential vorticity using the reversibility principle (Hoskins et al., 1985). Potential vorticity represents the combined effects of changes in wind direction and potential temperature vertical gradient during the storm evolution. It mirrors the vorticity production by baroclinic structures. Like potential temperature, the positive anomalies of potential vorticity induce cyclonic circulations, while negative anomalies correspond to anticyclonic circulations (Hoskins et al., 1985).

Thorncroft and Blackburn (1999) and Thorncroft et al. (2003) show that the weakness of the static stability in the atmospheric boundary layer results in very low potential vorticity in the middle layers. In August 2000, during the JET 2000 campaign performed in West Africa, they observed that north of the 15°N latitude, West Africa and East Atlantic are characterized by very low potential vorticity. These low values give birth over this area to negative deviation of potential vorticity associated with the north anticyclonic leg of the AEJ, while, around latitude 12.5°N, high values are observed with a maximum above the ocean, around 30°W. These results illustrate the interest of potential vorticity as a middle tropospheric layer parameter to quantify the stability of this area. That is why an index parameter for potential vorticity at 700 hPa was defined, namely:

$$IPV = PV_{700}. \quad (6)$$

Gray (1977, 1979) used the vertical vorticity (ξ) at 900 hPa. This parameter, however, does not characterize the AEJ instability linked to waves (Thorncroft and Blackburn, 1999). To preserve an information on the horizontal convergence of low level fluxes, however, parameter ξ taken at 925 hPa has been retained, namely:

$$ITV = \xi_{925} \times 10^5 + 5. \quad (7)$$

The absolute value of $\xi_{925} \times 10^5$ being smaller than 5 in the performed circulation, number 5 was added in order to avoid a sign change of our cyclogenesis index.

3.5. *Sea surface temperature*

Observations show that convective activity and rainfall over Sahel are influenced by sea surface temperature (SST) (Edward and Cook, 2001; Kingtse et al., 2001). Tropical convection increases when SST reaches about 26°C (Tompkins, 2001). Gautier and Zipser (1976) suggest that central cyclonic system motion depends on SST distribution. Kingtse et al. (2001) show that SST has a significant influence on the rainy season over Sahel and is pivotal in the development of tropical depressions.

For the definition of the present cyclogenesis index, the thermal energy released by ocean has not been considered because, during the summer season of the northern hemisphere, SST over the studied area does not vary strongly with values higher than 26°C. Consequently, this parameter does not seem to be a discriminating one with respect to the birth of cyclones over this basin.

Table 3

Units of the various parameter indices

Index	f	IQ	ICI	ITe	IRE	IPV	ITV	ICYC
Unit	s^{-1}	kg/kg	-	K	K	UPV	s^{-1}	UPV.K

UPV is the unit of potential vorticity ($K m^2 kg^{-1} s^{-1}$).

3.6. Cyclogenesis index

The proposed cyclogenesis index ICY is obtained by combining the above discussed parameters indices. ICY is written:

$$ICY = f \times IQ \times ICI \times \left(\frac{IPV}{5 - ITV} \right) \times (35 + IRE - ITe) \quad (8)$$

where f is the Coriolis parameter. Units of the various terms are given in Table 3. Conservation of a cyclonic circulation, which is a required condition of cyclogenesis supply, is linked with this index.

The proposed combination is similar to that of Gray (1977, 1979) with a simplification of the units. A linear combination would give qualitatively similar results since each term is such as to increase when cyclogenesis conditions strengthen.

4. Tests of parameter indices and cyclogenesis index

The computation of the parameter average for various cases of coast crossing MCS shows that the zonal variation is strongly affected by the simultaneous presence of two cyclonic perturbations at two different longitudes but around the same latitude. That is why the meridian variations of the various parameter indices is considered. These variations are taken at the longitude of $17.5^\circ W$, which is just west of the Sahelian Africa Coast, between latitude 2.5 and $25^\circ N$, that is from near the equator to the middle of Sahara. Variations are calculated on the day when the MCS cross the coast. The observed variations are compared to their mean for the month of August over 10 years, from 1990 to 1999. August is chosen because 60% of the cases studied are observed during this month. This is also the month when the convective activity is the strongest in the Sahelian Strip.

4.1. Humidity index

Fig. 4 displays the variation with latitude of the mean humidity index IQ and the deviation of IQ with respect to the 10-year average for the two eventualities (strengthening and weakening) of MCS evolution at coast crossing, with a distinction between the cases selected by radar and those selected from satellite data. Curves corresponding to radar or satellite selected cases present similar shapes. Deviation with respect to 10-year mean computed for radar selected cases shows that strengthening and weakening curves are anticorrelated. Curves for satellite selected cases (not presented for the sake of simplicity) are almost the same. What can be seen is that there is more humidity at middle tropospheric level in the case of strengthening than for weakening cases. Fig. 4a shows that at $15^\circ N$ (i.e. latitude of Dakar), IQ

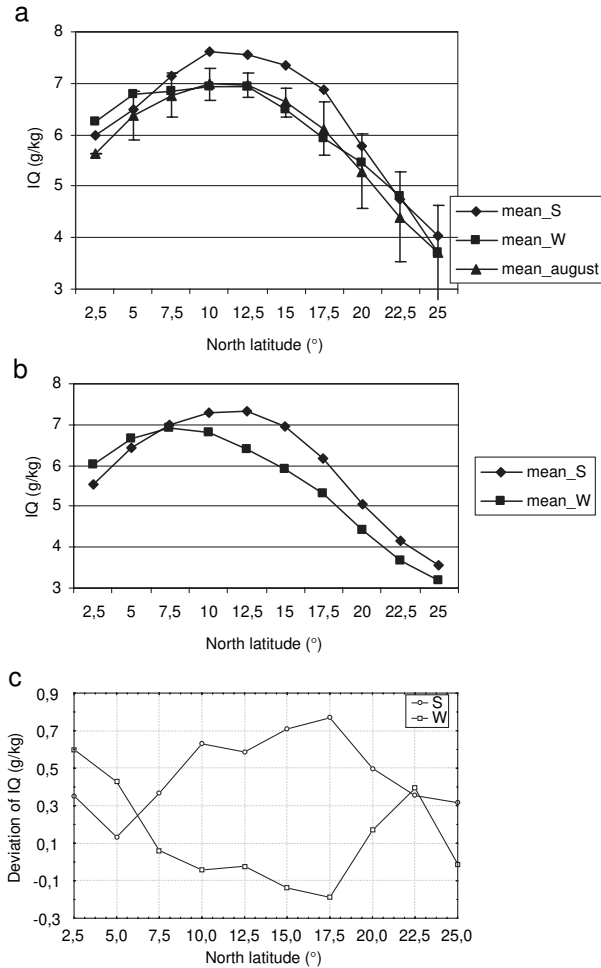


Fig. 4. Variation as a function of latitude of the humidity index IQ observed longitude 17.5°W and averaged over all the events of the corresponding category (strengthening—S or weakening—W). (a) displays the radar selected events and includes the mean for August. (b) shows the satellite selected events. (c) presents the deviation with respect to the 10-year average of each category. Vertical bars give the standard deviation with respect to the 10-year average for August.

for the strengthening case is about 7.4 g kg^{-1} , that is 10.6% higher than 10-year average which is 6.7 g kg^{-1} . In the case of weakening, the corresponding value is a 2.8% decrease.

4.2. Vertical wind shear index

Similarly with Fig. 4 for IQ, Fig. 5 displays the variation with respect to the latitude of the mean value and of the deviation with respect to the 10-year average of the vertical wind shear index ICI. The distribution of the deviation shows that, in the case of strengthening, the deviation is positive, that is the wind shear is smaller at all latitudes,

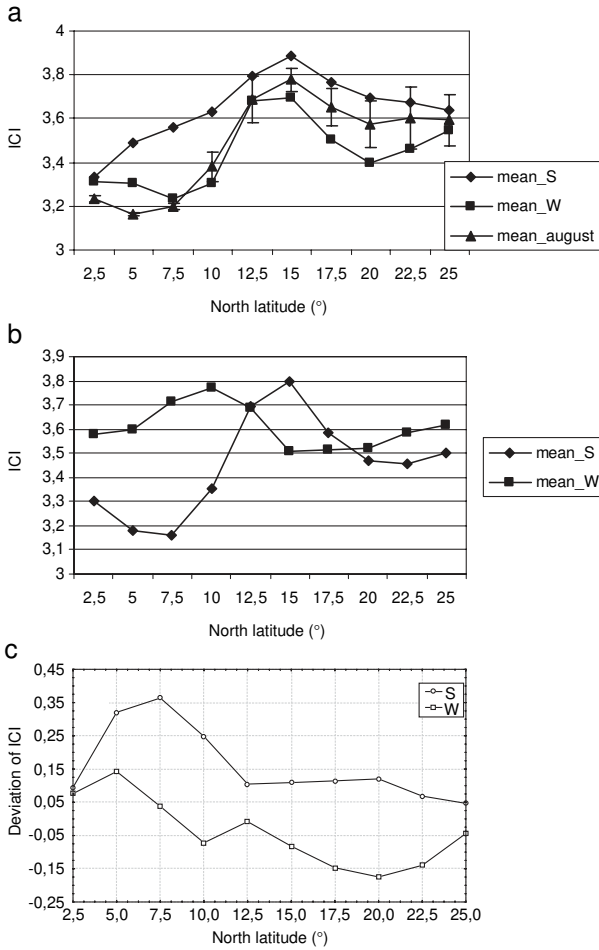


Fig. 5. Same as Fig. 4 but for the vertical wind shear index ICI.

with a constant value of about 0.1 between 12.5 and 20°N. At 15°N the 10-year average of ICI for August is 3.8, corresponding to a vertical wind shear of 3.89 m s^{-1} while when there is a strengthening, for strengthening case ICI=3.9, corresponding to a wind shear of 2.98 m s^{-1} . Deviation from the mean is larger between 5 and 7.5°N. At these latitudes the vertical wind shear for strengthening and weakening cases is 6.59 and 11.89 m s^{-1} , respectively, and the 10-year average is 12.76 m s^{-1} . Clearly, the vertical wind shear is small in the presence of a strengthening process. In this case ICI is observed to be increasing. In all the cases of MCS (i.e. strengthening or weakening), the vertical wind shear is rather low west of the Dakar latitude. For the MCS cases selected from satellite data, the vertical wind shear for weakening systems is smaller than for the strengthening ones for latitudes below 12.5°N. This can be due to the presence at these equatorial latitude of a convection stronger than at Sahelian latitudes, knowing that the convective activity tends to reduce the vertical wind shear by homogenizing the horizontal quantity of motion.

4.3. Warming index

The warming of upper layers (IRE) and decrease of equivalent potential temperature between low and middle layers (IT_e) are simultaneously considered. The word “warming” is used to refer to the combination of these two terms inside a warming index written $(35+IRE+ITE)$ where 35 is an arbitrary coefficient. Fig. 6 presents the variation of the warming index as a function of latitude in a way similar to what is shown in Fig. 4. Deviation with respect to the 10-year average (Fig. 6c) shows that the strengthening and weakening curves are anticorrelated, with, for each of them, a change of the sign around $13-15^\circ\text{N}$, that is at the coast crossing latitude.

Amplitude of index variations is much larger for strengthening than for weakening curves. Between 5 and 13°N , the deviation is positive with peak at 3.6 K for strengthening

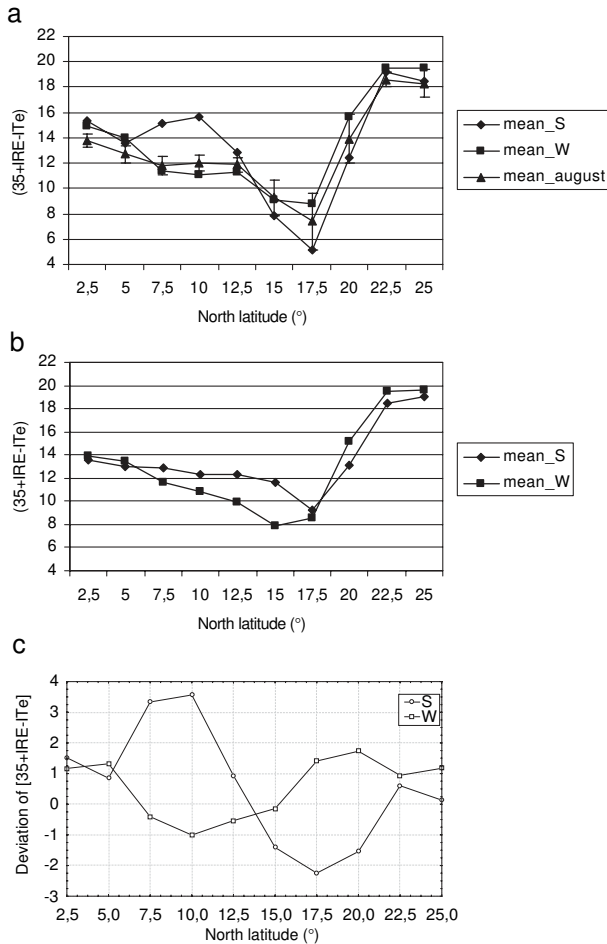


Fig. 6. Same as Fig. 4 but for the warming index $(35+IRE+ITE)$ where IRE and ITE are in K.

cases and a negative deviation peaking to -1 K for weakening cases. Between 15 and 22.5°N , the deviation is inverted with respect to the 5 – 13°N region. Observation shows that, west of the African Coast, the perturbation motion is mainly along a west to south–west direction. Fig. 6c suggests that the warming index distribution could be related with this evolution.

4.4. Vorticity index

The vorticity index is a combination of potential vorticity at middle level (IPV) and vertical vorticity at low level (ITV). It is written $(IPV/(5 - ITV))$ and mirrors the horizontal convergence of the low layer flux and the production of vorticity by baroclinic phenomena. The evolution of the mean value and of the 10-year average deviation as a function of the latitude is presented in Fig. 7. The deviations for strengthening and

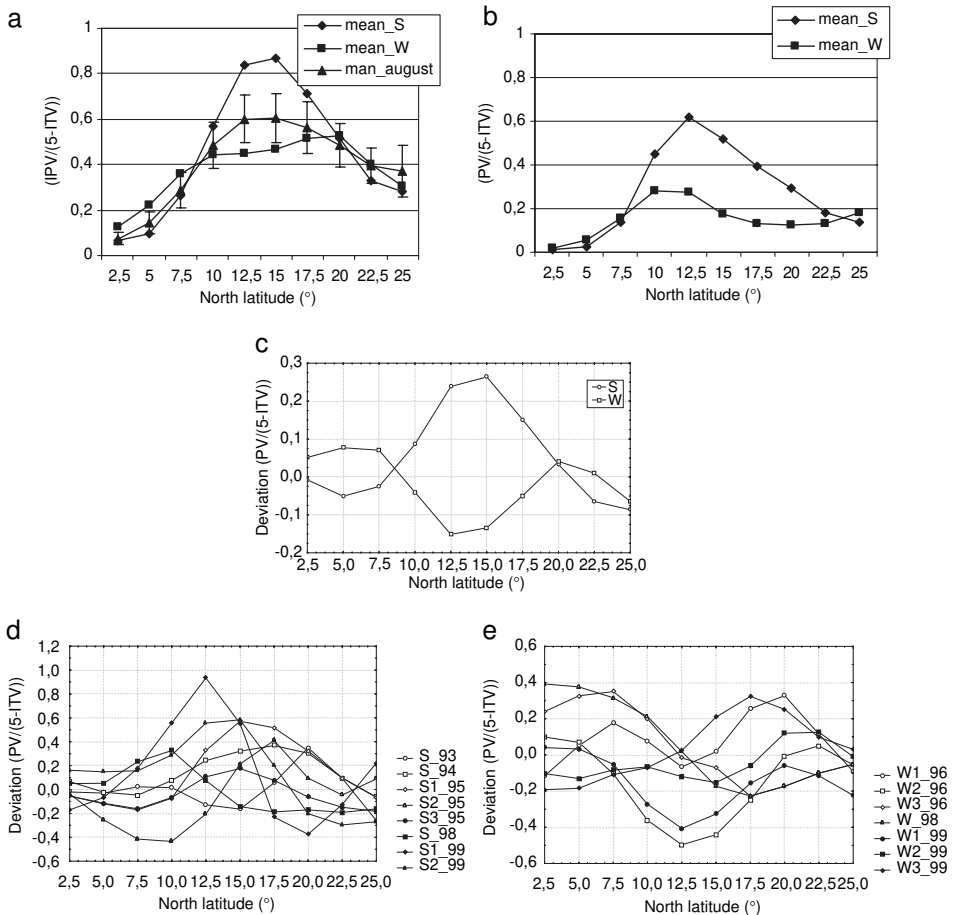


Fig. 7. Same as Fig. 4 but for the vorticity index $(PV/(5 - ITV))$ in unit of (UPV)s with UPV in $\text{K m}^2 \text{kg}^{-1} \text{s}^{-1}$. In addition, panels d and e display the deviation with respect to the 7-year average of individual events.

weakening cases are again clearly anticorrelated, with a stronger amplitude between about 10 and 20°N. The vorticity index is thus very discriminating between strengthening and weakening cases. Curves of vorticity index deviation for individual cases are displayed in Fig. 7c to support this statement.

4.5. Test of the cyclogenesis index

4.5.1. Spatio-temporal variation

Figs. 8a and b display the mean ICY as a function of latitude for radar and satellite selected cases (a and b, respectively). Between 10 and 20°N, the strengthening and weakening curves are nearby distinct, with peaks about three times higher for strengthening than for weakening. Figs. 8c and d display the variation of the deviation from 10 years average of ICY for strengthening and weakening individual events (Table 1)

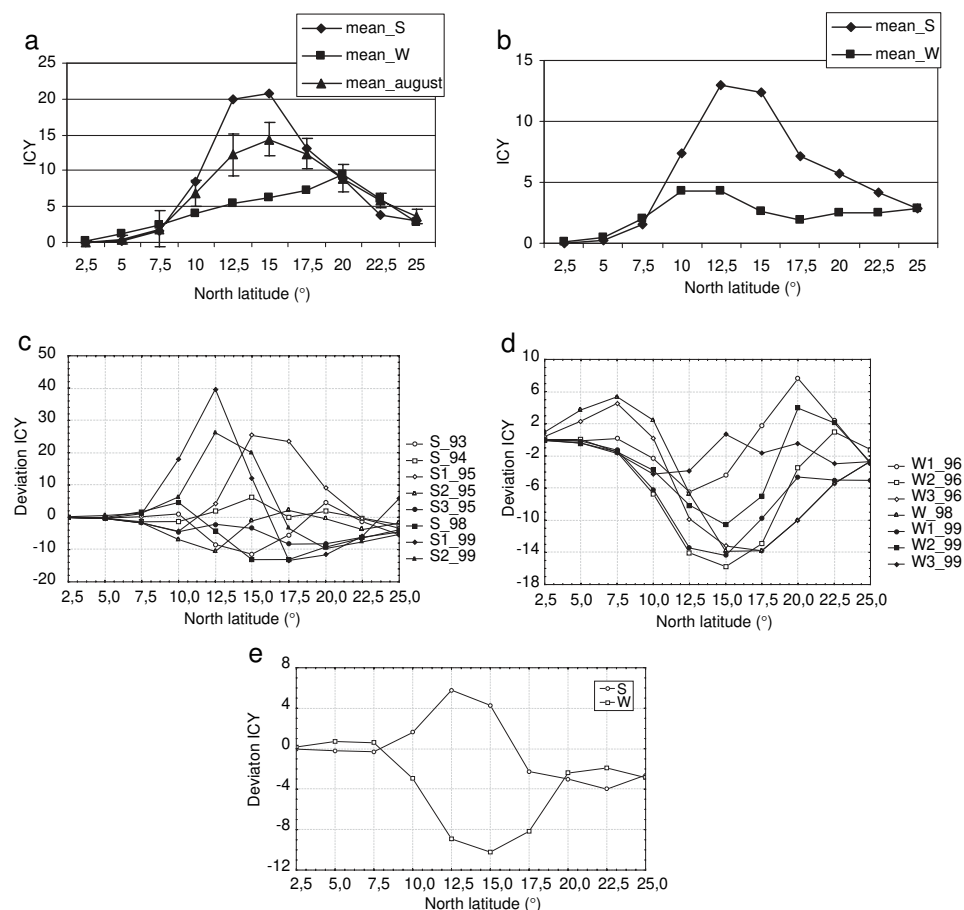


Fig. 8. Same as Fig. 4 but for the global index ICY in unit of (UPV)K. In addition panels c and d present the variation of deviation from the 10-year average of individual events. e gives the mean of c and d.

and Fig. 8e shows the mean curves deduced from c and d. For strengthening events (Fig. 8c), deviation is positive for four of the eight events around the MCS coast crossing latitude. For the weakening events (Fig. 8d), deviation is negative for all events. The mean curves (Fig. 8e) are strongly anticorrelated; between 10 and 15°N deviation for strengthening peaks at 6 UPV.K, around 12.5°N. The corresponding 10-year average for 14 UPV.K, that is an increase of about 63% with respect to the 10-year average. For the weakening case, the minimum of the deviation located at 15°N is -10 UPV.K with a 10-year average of 16.5 UPV.K, that is a decrease of 61%. These results show that ICY discriminates rather well the two classes of events.

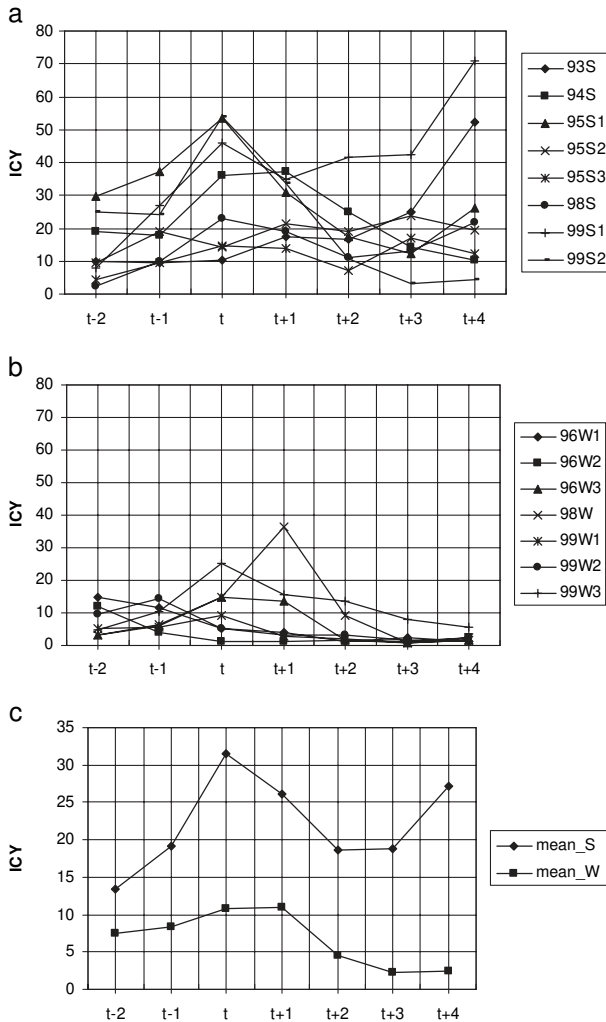


Fig. 9. Variation of ICY calculated in a frame linked to the system for individual events (a and b) and mean curves (c). t is the day of coast crossing, $t - 1$ is the day before coast crossing and so on.

To emphasize the coast crossing change, ICY was calculated in a frame linked to the MCS (Lagrangian) for each event selected by radar. The successive positions of MCS were noted with respect to the coast crossing day designed by t . ICY was computed as an average over nine cartesian grid points, one located the nearest of the MCS center and eight around this one, with a mesh of 2.5° .

Figs. 9a and b show, for each radar selected event, the variation of this space averaged ICY as a function time over 6 days, two before coast crossing and four after coast crossing. Time in abscissa can also be interpreted as giving the MCS distance from the Atlantic Coast, about 2000 km over land and 3000 km over sea. Fig. 9c shows the two mean curves corresponding to a and b. For the strengthening, case ICYC increases (by a factor 2 for the mean curve) between $t-2$ and t , then decreases between t and $t+2$, and increases again after $t+3$. For the weakening cases, the mean of ICY increases slightly between $t-2$ and t is constant between t and $t+1$ and decreases after $t+1$. For weakening cases, ICY is much smaller than for strengthening cases. Fig. 9c also emphasizes the three phases of the ICY variation for strengthening and the two phases of weakening cases.

4.5.2. Relation between ICY maximum and beginning of cyclogenesis

Fig. 10 displays the field of ICY computed for the day when four Africa-originated perturbations were, for the first time, classified as tropical depression by NHC. In addition, Fig. 10 gives the geographic location of the perturbation center at the time of the classification change. A clear coincidence between the maximum of ICY and the starting point of the tropical depression circulation.

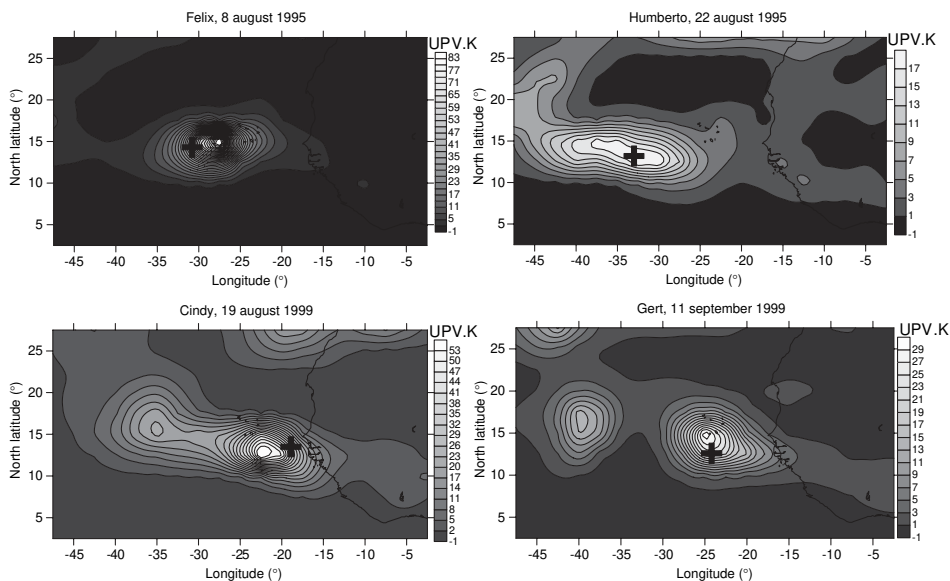


Fig. 10. Isolines of ICY and location of the convective system center at the time when they were classified as tropical depression by NHC (cross) for four tropical cyclones: Felix, Humberto, Cindy and Gert.

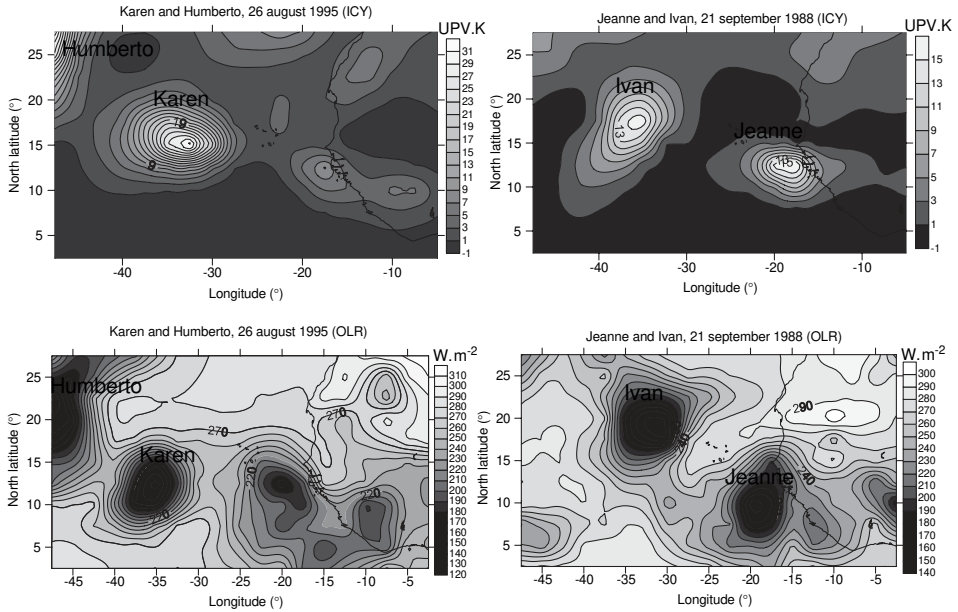


Fig. 11. Isolines of ICY and OLR for two events displaying simultaneously two cyclonic perturbations inside the analysed area showing the ability of ICY to discriminate the two systems.

Fig. 11 illustrates, for two events, the relation between ICY and OLR space distributions in the case when two cyclonic perturbations are simultaneously present in the studied area of Eastern Tropical Atlantic: on 26 August 1995, cyclones Karen and Humberto (at the limit of the area) and, on 21 September 1988 cyclones Ivan and Jeanne. What can be seen is that there is a good coincidence between the field of OLR associated with the cyclonic perturbation and the field of ICY. The field of ICY clearly discriminates the two simultaneous cyclonic systems.

In addition, to visualize the relation between ICY and cloud cover, Fig. 12 shows the time-longitude distribution of ICY and OLR at 15°N for August and September 1999 during which cyclones Cindy and Gert respectively happened. Cyclone Cindy is identified on 19 August 1999 around longitude 19°W and cyclone Gert on 11 September 1999 around longitude 24°W. OLR and ICY distributions are in agreement.

5. Conclusion

From dynamic and thermodynamic atmospheric parameters Gray (1977, 1979) has elaborated an index to describe the climatology of cyclogenesis area. Following a similar approach, an index intended to identify the cyclogenesis processes in the coast crossing Sahelian MCSs has been developed. The goal was to detect and discriminate the processes of strengthening or weakening affecting the MCSs after coast crossing and thus to detect cyclogenesis over Atlantic. In addition of parameters used by Gray (1977, 1979) which have been adapted to the context of the present study, other terms have been defined.

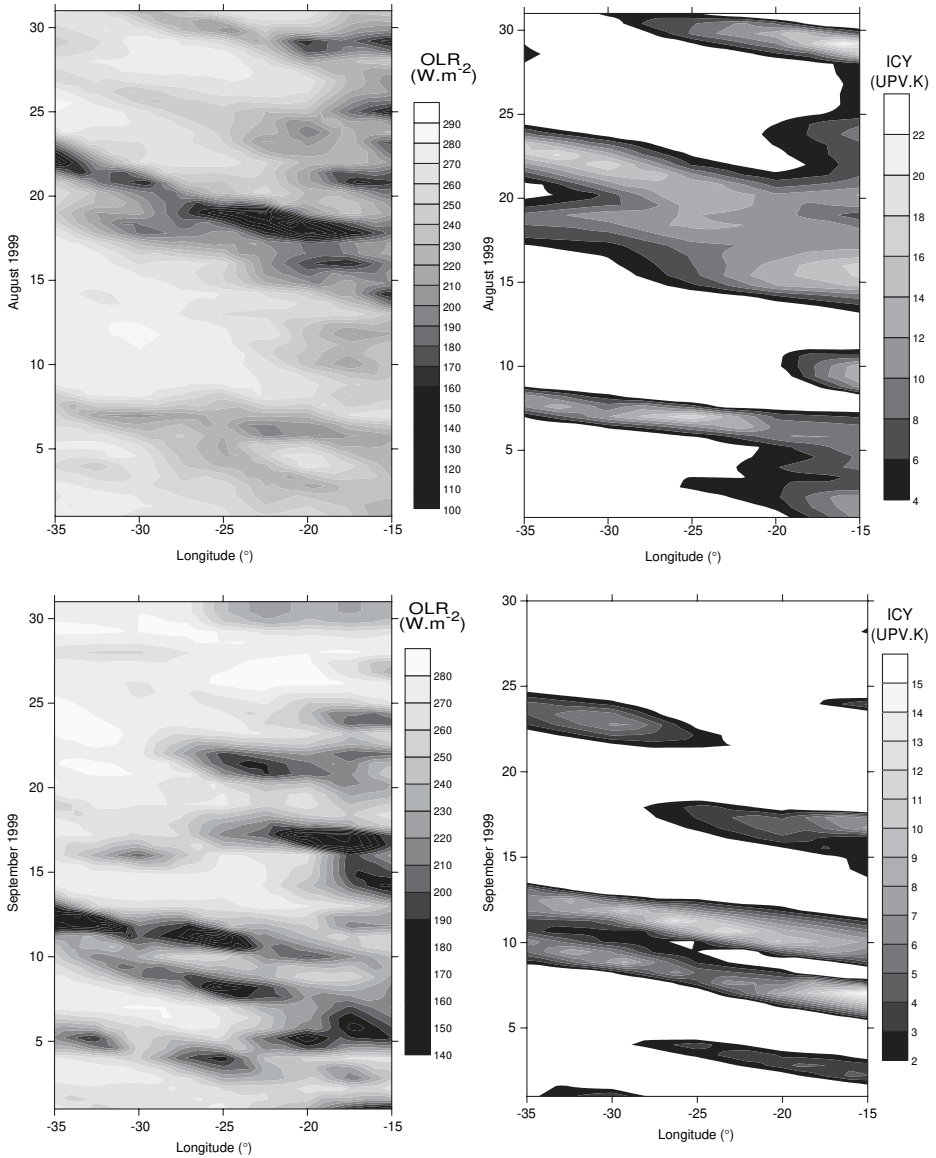


Fig. 12. Time–longitude chart of OLR and ICY for August and September 1999 showing the agreement between the distribution of the two terms.

Finally four combined parameter indices were defined to describe humidity, wind shear, warming and vorticity. These indices were gathered inside a cyclogenesis index ICY.

To test these various indices, fifteen coast crossing MCS were selected by radar, eight for strengthening and seven for weakening processes. To enlarge this first data set, 118 cases of MCS crossing the coast and then strengthening or weakening over the Atlantic

Ocean were identified from Meteosat satellite data and included in a complementary data set. The data used for the tests are mainly reanalyses of NCEP/NCAR, data on outgoing longwave radiation distribution, information from NHC, and data from Dakar-Yoff radar.

Analysis of meridian distribution of parameter indices calculated for the MCS coast crossing time shows that parameter provided by the combination between vertical vorticity at 925 hPa (accounting for low level convergence) and potential vorticity at 700 hPa (accounting for instability in midlevel layer) discriminate efficiently between strengthening and weakening evolution offshore near the African Coast. Between 10°N and 17.5°N, the deviation with respect to 10-year average of this parameter index for strengthening and weakening cases are anticorrelated. This anticorrelated deviation appears clearly on the curves of the individual events. For the other indices, an anticorrelation of the mean curves for the two classes of case is also observed, notably for ICY which is strongly differentiated between latitude 10°N and 17.5°N. Time or zonal variation of the ICY mean, using a Lagrangian coordinate reference, shows this index is much larger for strengthening than for weakening class.

The maximum of ICY has been shown to coincide with the starting of the cyclogenesis process as defined from the classification of the perturbation as tropical depression. ICY also appears to be able to discriminate two cyclonic perturbations simultaneously present in the East part of the Atlantic Ocean. In addition, the space distribution and the time-longitude distribution of ICY and OLR are found in good agreement.

All these results suggest that ICY deserves to be considered for the identification cyclogenesis processes.

Acknowledgments

The authors thank the Agence Universitaire de la Francophonie (AUF) for funding the stay in France of one of them (SMS). They are also grateful to the National Centers for Environmental Prediction/National Center for Atmospheric Research, to the National Hurricane Center for making their data available to them, to the Direction de la Météorologie du Sénégal and to the Agence pour la Sécurité de la Navigation Aérienne for providing the data from Senegal. Many thanks also to the team of Laboratoire de Physique de l'Atmosphère Simeon Fongang of the University Cheikh Anta Diop of Dakar for radar handling between 1993 and 1999.

References

- Arbogast, P., 2002. L'inversion du tourbillon potentiel, un outil pour comprendre le creusement des dépressions. *La Météorologie*, 8^{ème} série 38, 19–29.
- Arkin, P.A., 1979. The relationship between fractional coverage of high cloud and rainfall accumulations during GATE over the B-scale array. *Mon. Weather Rev.* 107, 1382–1387.
- Arkin, P.A., Meisner, B., 1987. The relationship between large-scale convective rainfall and cold cloud over the Western hemisphere during 1982–1984. *Mon. Weather Rev.* 115, 51–74.
- Arnaud, Y., Desbois, M., Maizi, J., 1992. Automatic Tracking and characterization of African convective systems on Meteosat pictures. *J. Appl. Meteorol.* 31, 443–453.

- Aspliden, C.I., Adefolalu, D., 1976. The mean troposphere of West Africa. *J. Appl. Meteorol.* 15, 705–716.
- Balasubramanian, G., Yau, M.K., 1996. The life cycle of the simulated marine cyclone: energetics and PV diagnostics. *J. Atmos. Sci.* 53, 639–653.
- Bartels, D.L., Maddox, R.A., 1991. Midlevel cyclonic vortices generated by mesoscale convective systems. *Mon. Weather Rev.* 119, 104–118.
- Burpee, R.W., 1972. The origin and structure of easterly waves in the lower troposphere of North Africa. *J. Atmos. Sci.* 29, 77–90.
- Cadet, D.L., Nnoli, N.O., 1987. Water vapor transport over Africa and the Atlantic Ocean during summer 1979. *Q. J. Royal Meteorol. Soc.* 113, 581–602.
- Calheiros, R.V., Zawadzki, I., 1987. Reflectivity–rain rate relationships for radar hydrology in Brazil. *J. Clim. Appl. Meteorol.* 26, 118–132.
- Charney, J.G., Stern, M.E., 1962. On the stability of internal baroclinic jets in a rotating atmosphere. *J. Atmos. Sci.* 19, 159–172.
- De Félice, P., Viltard, A., Camara, M., 1982. Vapeur d'eau dans la troposphère en Afrique de l'Ouest. *La Météorologie* 29 (VI^e série), 129–133.
- De Félice, P., Viltard, A., Oubuih, J., 1993. A synoptic-scale wave of 6–9 day period in the Atlantic tropical troposphere during summer 1981. *Mon. Weather Rev.* 121, 1291–1298.
- DeMaria, M., 1996. The effect of vertical shear on tropical cyclone intensity change. *J. Atmos. Sci.* 53, 2076–2087.
- DeMaria, M., Knaff, J.A., Connell, B.H., 2001. A tropical cyclone genesis parameter for the tropical Atlantic. *Weather Forecast* 16, 219–233.
- Deme, A., Viltard, A., de Félice, P., 2003. Daily precipitation forecasting in Dakar using the NCEP-NCAR reanalyses. *Weather Forecast* 18, 93–105.
- Diedhiou, A., Janicot, S., Viltard, A., de Félice, P., 1998. Evidence on two regimes of easterly wave over West Africa and the tropical Atlantic. *Geophys. Res. Lett.* 25, 2805–2808.
- Diedhiou, A., Janicot, S., Viltard, A., de Félice, P., Laurent, H., 1999. Easterly wave regimes and associated convection over West Africa and Tropical Atlantic: results from the NCEP/NCAR and ECMWF reanalyses. *Clim. Dyn.* 15, 795–822.
- Edward, K., Cook, K.H., 2001. Mechanisms by which Gulf of Guinea and Eastern North Atlantic Sea surface temperature anomalies can influence African rainfall. *J. Climate* 14, 795–821.
- Emanuel, K.A., Renno, N., Schade, L.R., Bister, M., Morgan, M., Raymond, D.J., Rotunno, R., 1993. Tropical cyclogenesis over the Eastern North Pacific: some results from the texmex. 20th Conf. On Hurricane and Tropical Meteorology. Amer. Meteor. Soc., San Antonio (TX, US), pp. 110–113.
- Frank, W.M., 1987. Tropical cyclone formation. In: Elsberry, R.L. (Ed.), *A Global View of Tropical Cyclones*. Naval Postgraduate School, pp. 53–90.
- Gautier, C., Zipser, E., 1976. Convection and wind structure in a GATE depression. 10th Tech. Conf. Hurricanes and Tropical Meteorology, Charlottesville, July 1976.
- Gray, W.M., 1968. Global view of the origin of tropical disturbances and storms. *Mon. Weather Rev.* 96, 669–770.
- Gray, W.M., 1977. Tropical cyclone genesis in the western North Pacific. *J. Meteorol. Soc. Jpn.* 55, 465–482.
- Gray, W.M., 1979. Hurricanes: their formation, structure and likely role in the tropical circulation. In: Shaw, D.B. (Ed.), *Meteorology over the Tropical Oceans*. Roy. Meteor. Soc., pp. 155–218.
- Gray, W.M., 1990. Strong association between West African rainfall and US landfall of intense hurricanes. *Science* 249, 1251–1256.
- Gray, W.M., Landsea, C.W., 1992. African rainfall as a precursor of hurricane-related destruction on the US East Coast. *Bull. Am. Meteorol. Soc.* 73, 1352–1364.
- Gray, W.M., Landsea, C.W., Mielke Jr., P.W., Berry, K.J., 1994. Predicting Atlantic seasonal tropical cyclone activity by 1 June. *Weather Forecast.* 9, 103–115.
- Gray, W.M., Landsea, C.W., Mielke Jr., P.W., Berry, K.J., 1999. Forecast of Atlantic seasonal hurricane activity for 1999. Dept. of Atmos. Sci. Report, Colo. State Univ., Ft. Collins, CO, released on 4 June, 1999.
- Grist, J.P., Nicholson, S.A., 2001. A study of the dynamic factors influencing the variability of rainfall in the West African Sahel. *J. Climate* 14, 1337–1359.

- Harr, P.A., Elsberry, R.L., Chan, C.L., 1996. Transformation of a large monsoon depression to a tropical storm during TCM-93. *Mon. Weather Rev.* 124, 2625–2643.
- Hoskins, B.J., McIntyre, M.E., Robertson, R.W., 1985. On the use and significance of isentropic potential vorticity maps. *Q. J. Royal Meteorol. Soc.* 111, 877–946.
- Houze Jr., R.A., Betts, A.K., 1981. Convection in GATE. *Rev. Geophys. Space Phys.* 19, 541–576.
- Kalnay, E., Kanamitsu, M., Kistler, R., Collins, W., et al., 1996. The NCEP/NCAR 40-year reanalysis project. *Bull. Am. Meteorol. Soc.* 77, 437–471.
- Kebe, C.M.F., Sauvageot, H., Nzeukou, A., in press. The relation between rainfall and area-time integrals at the transition from an arid to an equatorial climate. *J. Clim.*
- Kingtse, M., Gerald, D.B., Thiaw, W.M., 2001. Impact of sea surface temperature anomalies on the Atlantic tropical storm activity and West African rainfall. *J. Atmos. Sci.* 58, 3477–3496.
- Laing, A.G., Fritsch, J.M., Negri, A.J., 1999. Contribution of mesoscale convective complexes to rainfall in Sahelian Africa: estimates from geostationary infrared and passive microwave data. *J. Appl. Meteorol.* 38, 957–964.
- Lamb, P.J., 1983. West African water vapor variations between recent contrasting Sub-Saharan rainy seasons. *Tellus* 35A, 198–212.
- Landsea, C.W., Bell, G.D., Gray, W.M., Goldenberg, S.B., 1998. The extremely active 1995 Atlantic hurricane season: environmental conditions and verification of seasonal forecasts. *Mon. Weather Rev.* 126, 1174–1193.
- Landsea, C.W., Pielke Jr., R.A., Mestas-Nunez, A.M., Knaff, J.A., 1999. Atlantic basin hurricanes: indices of climatic changes. *Clim. Change* 42, 89–129.
- Laurent, H., 1996. Life distribution of mesoscale convective clouds over Africa. Preprints 7th Conf. on Mesoscale Processes. Amer. Meteor. Soc., Reading, UK, pp. 9–13.
- Laurent, H., D'Amato, N., Lebel, T., 1998. How important is the contribution of the mesoscale convective complexes to the Sahelian rainfall? *Phys. Chem. Earth* 23, 629–633.
- Lawrence, M.B., Avila, L.A., Beven, J.L., Franklin, J.L., Guiney, J.L., Pasch, R.J., 2001. Atlantic hurricane season of 1999. *Mon. Weather Rev.* 129, 3057–3084.
- Mathon, V., Laurent, H., 2001. Life cycle of Sahelian mesoscale convective cloud systems. *Q. J. R. Meteorol. Soc.* 127, 377–406.
- McBride, J.L., 1981. Observational analysis of tropical cyclone formation: Part I. Basic description of data sets. *J. Atmos. Sci.* 38, 1117–1131.
- McBride, J.L., Zehr, R., 1981. Observational analysis of tropical cyclone formation: Part II. Comparison of non-developing versus developing systems. *J. Atmos. Sci.* 38, 1132–1151.
- Molinari, J., Moore, P.K., Idone, V.P., Henderson, R.W., Saljoughy, A.B., 1994. Cloud-to-ground lightning in Hurricane Andrew. *J. Geophys. Res.*, 16665–16676.
- Nicholson, S.E., Grist, J.P., 2003. The seasonal evolution of the atmospheric circulation over West Africa and Equatorial Africa. *J. Climate* 7, 1013–1030.
- Nzeukou, A., Sauvageot, H., 2002. Distribution of rainfall parameters near the Coasts of France and Senegal. *J. Appl. Meteorol.* 41, 69–82.
- Nzeukou, A., Sauvageot, H., Ochou, A.D., Kebe, C.M.F., 2004. Raindrop size distribution and radar parameters at Cape Verde. *J. Appl. Meteorol.* 43, 90–105.
- Reed, R.J., Norquist, D.C., Recker, E.E., 1977. The structure and properties of African wave disturbances as observed during phase III of GATE. *Mon. Weather Rev.* 105, 317–333.
- Richards, F., Arkin, P.A., 1981. On the relationship between satellite-observed cloud cover and precipitation. *Mon. Weather Rev.* 109, 1081–1093.
- Sall, S.M., 1997. Interaction entre les ondes tropicales et les systèmes convectifs sur l'Afrique de l'Ouest durant l'été des années 1990, 1993 et 1994. Thèse de Docteur-Ingénieur, ESP, Univ. C.A. Diop de Dakar, 131 pp.
- Sall, S.M., Sauvageot, H., in press. Cyclogenesis off the African Coast: the case of Cindy in August 1999. *Mon. Weather Rev.*
- Sarr, A., Fongang, S., Sauvageot, H., 1995. Etude d'un indice énergétique de prévision de lignes de grains à Dakar. *Sécheresse* 6, 337–346.
- Simpson, R.H., 1974. The hurricane disaster potential scale. *Weatherwise* 27, 169–186.
- Thorncroft, C.D., Blackburn, M., 1999. Maintenance of the African easterly jet. *Q. J. Royal Meteorol. Soc.* 125, 763–786.

- Thorncroft, C.D., Hodges, K.I., 2001. African easterly wave variability and its relationship to Atlantic tropical cyclone activity. *J. Climate* 14, 1166–1179.
- Thorncroft, C.D., Parker, D.J., Burton, R.R., Diop, M., Ayers, J.H., Barjat, H., Devereau, S., Diongue, A., Dumelow, R., Kindred, D.R., Price, N.M., Saloum, M., Taylor, C.M., Tompkins, A.M., 2003. The JET200 project. *Bull. Am. Meteorol. Soc.* 84, 337–351.
- Tompkins, A.M., 2001. On the relationship between tropical convection and sea surface temperature. *J. Climate* 14, 633–637.
- Wayne, C.B., Colucci, S.J., 1996. A forecast and analyzed cyclogenesis event diagnosed with potential vorticity. *Mon. Weather Rev.* 124, 2227–2244.